

Effect of Yb³⁺ concentration on microstructure and optical properties of Yb: SrF₂ transparent ceramics

Yiwei Gao^a, Bingchu Mei^{a,*}, Weiwei Li^{a,**}, Zhiwei Zhou^a, Zuodong Liu^b

^a State Key Laboratory of Advanced Technology for Materials Synthesis and Processing, Wuhan University of Technology, Wuhan, 430070, China

^b Henan Key Laboratory of Utilization of Non-metallic Mineral in the South of Henan, Xinyang Normal University, Xinyang, China

ARTICLE INFO

Keywords:

Ytterbium
Fluoride strontium
Spectral property
Transparent ceramic

ABSTRACT

Ytterbium-doped strontium fluoride (Yb: SrF₂) nanopowders with different amounts of Yb³⁺ were synthesized by a co-precipitation method. XRD and FE-SEM measurements were used to characterize the phase composition and morphologies of these nanopowders. The Yb: SrF₂ nanopowders doped with 1–5 at.% Yb³⁺ showed the same phase as pure SrF₂, with a mean particle size of 20 nm. Transparent Yb: SrF₂ ceramics were fabricated by hot-pressing the nanopowders, and the transmittance of 1 at.% Yb: SrF₂ with a thickness of 2 mm was 85% at 1200 nm. The absorption spectra, luminescence spectra, and luminescence decays of the ceramics were also obtained. As the Yb³⁺ doping amount increased, the absorption and emission intensities also increased, indicating the absence of a concentration quenching effect in the Yb: SrF₂ ceramics. However, the decay lifetimes decreased with increasing Yb³⁺ content, and 1–5% Yb: SrF₂ transparent ceramics had decay lifetimes of 4.58, 3.48, 3.22, and 3.19 ms, respectively.

1. Introduction

Due to the emergence of LD pump sources with long lifetimes and high efficiencies [1], Yb³⁺ activated materials have been explored. The electron configuration of Yb³⁺ is [Xe]4f¹³ and it has only two electronic states, the ground state ²F_{7/2} and the excited state ²F_{5/2} [2–4], which can prevent laser energy loss due to up-conversion, excitation state absorption, and relaxation oscillation [5,6]. Since the absorption band of Yb³⁺ is located at 900–1000 nm, it can effectively couple with the InGaAs diode pump source without the need to strictly control the laser diode temperature [7]. Yb³⁺ is expected to replace neodymium-doped laser materials as the preferred solid laser gain medium for LD pumped high-efficiency and high-power lasers due to its lower thermal effect and concentration quenching and higher fluorescence lifetime compared with activated ions such as Nd³⁺ [8,9]. In addition, Yb³⁺ ions have longer fluorescence lifetimes, broader absorption, and emission bands in ultra-short laser generation and mode-locked pulse generation compared with other rare-earth ions. Yb³⁺ is also a highly efficient sensitizing ion that can be used as a pump energy absorption sensitizing agent for various laser-activated ions [10–12].

In 1971, Reinberg et al. obtained the first pulse laser output of 1.029

μm with a GaAs light-emitting diode pumped Yb: YAG crystal doped with Si [13], but further developments were temporarily abandoned because of its poor beam quality and laser efficiency. In 1991, Lacorvara et al. reported an InGaAs diode pumped Yb: YAG crystal which produced a continuous laser output at room temperature. The absorption pump power was 245 mW, and the maximum output power of 23 mW [14]. The current hosts for Yb³⁺ ions are YAG and other oxide materials; however, compared with oxide matrixes, fluorine materials have many advantages such as wide transmission wavelength ranges, low phonon energies, low refractive indexes, and low melting points. SrF₂ shows better properties than CaF₂, and has a larger lattice parameter, which weakens interactions between Yb³⁺ ions and interstitial F⁻ ions [15–17]. The critical concentration causing Yb³⁺ ions to cluster with each other is higher in SrF₂, which leads to a weaker concentration quenching effect in SrF₂, allowing higher Yb³⁺ doping concentration. Moreover, the absorption cross-section and fluorescence lifetime of Yb³⁺ in SrF₂ are both larger than in CaF₂ [18,19]. Unfortunately, there are few literature reports that emphasize the fabrication of highly-transparent rare-earth doped SrF₂ ceramics. Moreover, there is a lack of studies which have explored the effects of Yb³⁺ doping concentration on the microstructure and optical properties of ceramics.

* Corresponding author.

** Corresponding author.

E-mail addresses: bcmeilab@163.com (B. Mei), leeww@whut.edu.cn (W. Li).

<https://doi.org/10.1016/j.optmat.2020.109869>

Received 5 December 2019; Received in revised form 22 February 2020; Accepted 30 March 2020

Available online 16 April 2020

0925-3467/© 2020 Elsevier B.V. All rights reserved.

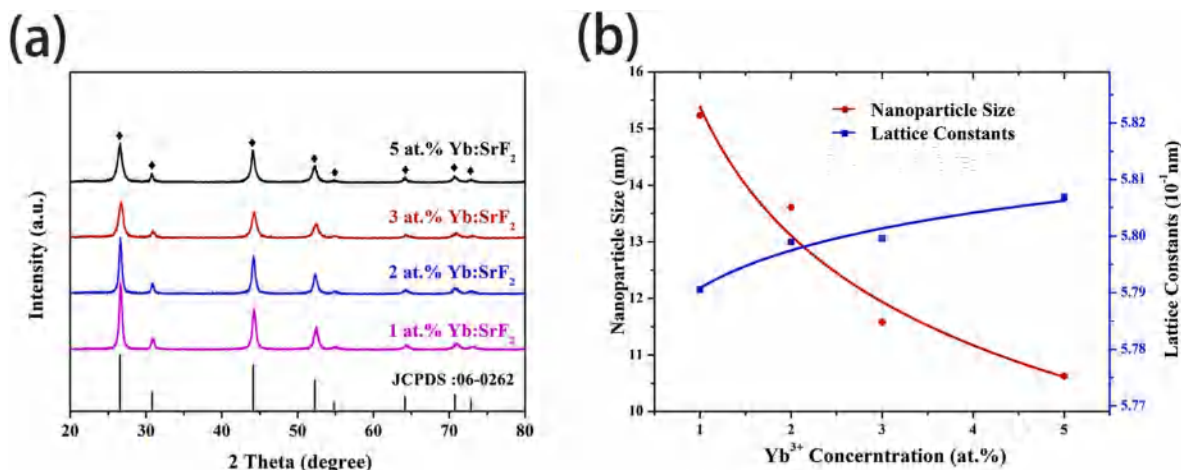


Fig. 1. XRD patterns of SrF₂ nanoparticles with different Yb doping concentrations (a), and nanoparticle sizes and lattice constants versus Yb doping concentration (b).

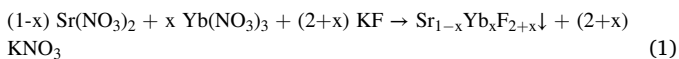
In this work, Yb: SrF₂ nanopowders with different Yb³⁺ doping concentrations were synthesized using a wet chemical co-precipitation method. FE-SEM and XRD measurements were used to characterize the phase and microstructure of these nanopowders. Transparent Yb: SrF₂ laser ceramics were fabricated by vacuum hot-pressing the obtained nanopowders. The influence of Yb³⁺ content on the microstructure and optical properties of the Yb: SrF₂ transparent ceramics were investigated.

2. Experimental

2.1. Materials and preparations

The Yb: SrF₂ nanopowders were prepared via a wet chemical co-precipitation method using commercial raw materials: hydrated strontium nitrate (Sr(NO₃)₂, >99.9% purity, Sinopharm), ytterbium nitrate (Yb(NO₃)₂·5H₂O, >99.9% purity, Aladdin), and hydrated potassium fluoride (KF·2H₂O, >99.9% purity, Sinopharm). All reagents were of analytical grade.

The cationic solution (Sr²⁺ and Yb³⁺) and anionic solution (F⁻) were prepared by dissolving nitrate salts and hydrated potassium fluoride in deionized water, respectively. After stirring these two solutions for 10 min, the mixed solution of strontium nitrate and ytterbium nitrate was slowly poured into the potassium fluoride solution and then magnetically stirred. The chemical equation of the reaction which occurs upon mixing is:



where x is the doping level ($x = 1, 2, 3,$ or 5 at.%). The mixed solution was stirred for 30 min and stored for 4 h at room temperature, and then centrifuged at 11,000 rpm for 15 min. The obtained precipitate was washed with distilled water to remove residual impurities. After repeating the centrifugation and washing processes 3 times, the precipitate was dried at 80 °C in an oven for 24 h. Finally, the Yb: SrF₂ nanopowders were obtained after being crushed in an agate mortar.

Yb: SrF₂ transparent ceramics were prepared through a hot-pressing and sintering method. The obtained powders were filled into a graphite mold with a 16 mm cavity diameter. Then, the powders were sintered at 800 °C with a heating rate of 10 °C/min and an axial pressure of 30 MPa. The sintering time was 2 h under a vacuum of 10⁻³ Pa. The obtained Yb: SrF₂ ceramic samples were polished into 2 mm for further characterization.

2.2. Measurements

The phase composition of the powders was determined by X-ray diffraction (XRD, Model D/Max-RB, Rigaku, Japan) in a 2θ range of 20°–80° using nickel-filtered Cu-Kα radiation ($\lambda = 1.5406$ Å). The powder morphologies and the microstructure of the ceramic fracture surfaces were observed by a field emission scanning electron microscope (FE-SEM; Zeiss Ultra Plus, German). The absorption spectra and in-line transmittance spectra of the transparent ceramics were measured using a spectrophotometer (Lambda-750, PerkinElmer, USA).

The emission and luminescence decay curves were measured using an Edinburgh Instruments FLS1000 fluorescence spectrometer. The emission spectra were excited at 896 nm equipped with a 450W Xenon source lamp. The fluorescence curves were recorded by taking a 60 W μs flash lamp (Edinburgh, μF900) as the exciting source with an NIR PMT (Hamamatsu, R5509-73) as the detector. All the data were collected in air at room temperature.

3. Results and discussion

Fig. 1 presents the XRD patterns of Yb: SrF₂ nanopowders doped with different Yb³⁺ concentrations. The Yb: SrF₂ nanopowders doped with 1–5 at.% Yb³⁺ retained the same diffraction peaks as pure SrF₂ (JCPDS file No. 06–0262).

During co-precipitation, the solubility equilibria of components ($K_{sp}(\text{SrF}_2) = 4.33 \times 10^{-9}$, $K_{sp}(\text{YbF}_3) = 1 \times 10^{-15}$) and Ostwald ripening of precipitates must be considered [20,21]. A possible growth mechanism is proposed based on the composition of the obtained Yb: SrF₂ raw powder. First, the precursor was converted to SrF₂ and YbF₃ nuclei during the nucleation stage. Subsequently, the nuclei grew to rudimentary nanopowders, and the larger SrF₂ nanoparticles grew by adsorbing the smaller YbF₃ particles on their surface. Then, Ostwald ripening occurred until well-crystallized Yb: SrF₂ nanopowders were formed. Therefore, this process can be described as “Nucleation/Crystallization/Ostwald ripening”.

As the Yb³⁺ doping concentration increased, the peak shapes became shorter and broader, suggesting a decrease in the crystallinity and size of the Yb: SrF₂ particles. The peak positions remained in nearly same locations in all four Yb: SrF₂ samples, indicating that changing the Yb³⁺ doping concentration (1–5 at.%) had little influence on the lattice constant. This phenomenon is different from Yb: CaF₂, whose peak positions typically shift to lower angles with increasing Yb³⁺ content. This can be explained by examining Nd: SrF₂ in the literature [15]. There are two opposing effects related to changes in the lattice constant of Yb: SrF₂. One is the substitution of smaller Yb³⁺ with larger Sr²⁺

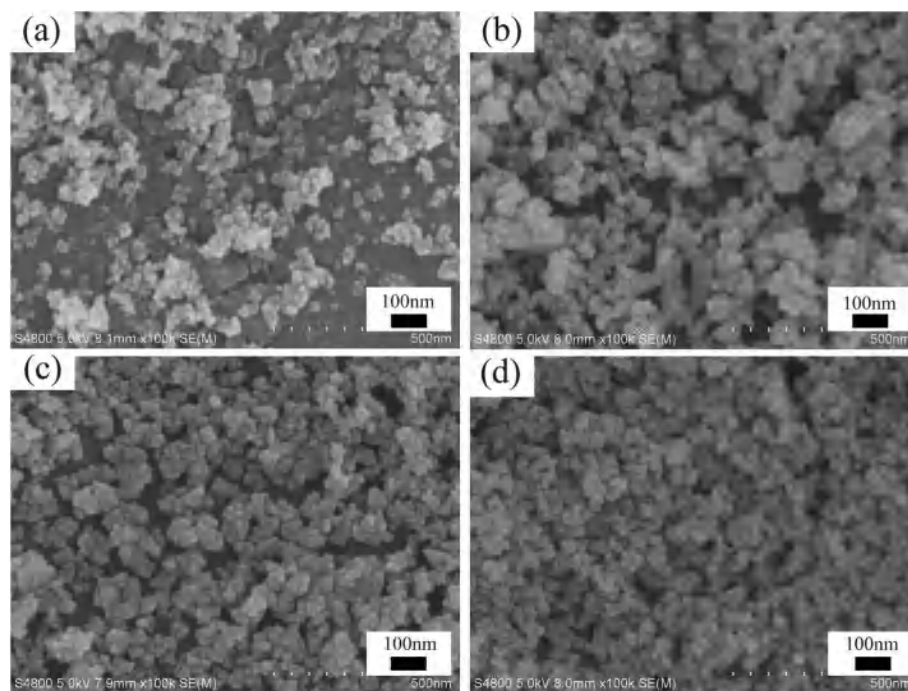


Fig. 2. FE-SEM images of Yb: SrF₂ nanopowders with different Yb doping concentrations: (a) 1 at.%, (b) 2 at.%, (c) 3 at.%, and (d) 5 at.%.

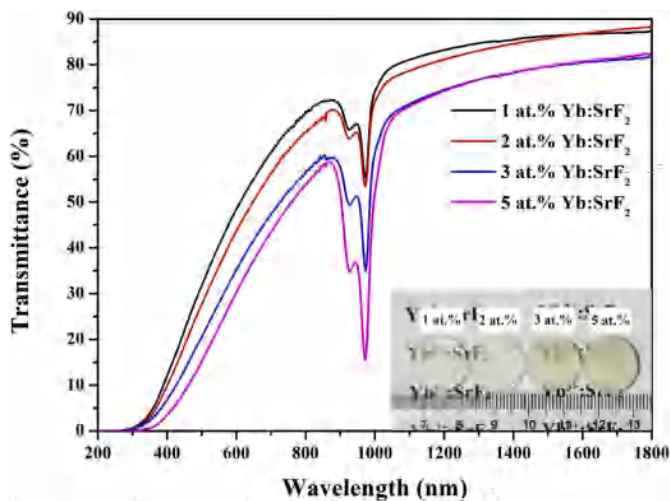


Fig. 3. Transmittance curves of the 1–5 at.% Yb: SrF₂ ceramics and photograph of mirror-polished ceramic samples obtained using the HP method.

(eight-coordinate radii: Yb³⁺ is 112.5 p.m.; Sr²⁺ is 140 p.m.), which shrinks the SrF₂ lattice. The other is the repulsion between charges compensating F⁻ and regular F⁻, which enlarges the lattice. These two opposing effects cancel each other out, resulting in nearly identical XRD peak positions. In the case of Yb: CaF₂, the lattice enlarging effect may dominate changes in the lattice constant because Ca²⁺ (126 p.m.) is smaller than Sr²⁺, which results in a weaker lattice shrinking effect. Consequently, with increasing Yb³⁺ doping concentration in Yb: CaF₂, more charge-compensating F⁻ ions will enter the interstitial sites. Therefore, the repulsion caused by the F⁻ is enhanced, resulting in a shift to lower angles in the XRD patterns. Fig. 1b plots the trend of calculated average particle sizes and lattice constants of Yb: SrF₂ against Yb³⁺ doping concentration. The average sizes and lattice constants range from 16 to 10 nm and 5.790–5.808 Å, respectively.

The FE-SEM micrographs in Fig. 2 show that most particles have a spherical morphology and with a mean size of 20 nm with a very low

agglomeration degree. The microstructure of the Yb: SrF₂ nanoparticles were very similar to Nd: SrF₂ reported in the literature [15]. Additionally, these FE-SEM images show a decreasing particle size versus Yb³⁺ doping concentration, which is in agreement with the XRD results (Fig. 1a and b).

Yb: SrF₂ transparent ceramics were fabricated by hot-pressing method the above nanopowders at 800 °C for 90 min under vacuum. The in-line transmittance spectra of the Yb: SrF₂ transparent ceramics are displayed in Fig. 3. The inset shows the appearance of particles with a 2 mm thickness and 16 mm diameter. Both sides of the samples were mechanically polished. The Yb: SrF₂ ceramics had good optical transparency, as the words placed under the samples can be clearly read.

The transmittance of ceramic samples doped with 1 at.% Yb: SrF₂ and 2 at.% Yb: SrF₂ samples was higher than that of 3 at.% Yb: SrF₂ and 5 at.% Yb: SrF₂ samples. The 1 at.% Yb: SrF₂ ceramic possessed the highest optical transmittance of 85% at 1200 nm. According to an earlier study [22,23], the theoretical highest transmittance of an SrF₂ transparent ceramic was 93.66%. The large difference between the transmittance of the highest transmittance of the Yb: SrF₂ ceramic in this work and the theoretical highest transmittance of SrF₂ ceramics indicates that optical losses occurred in the Yb: SrF₂ ceramics. Residual pores and grain boundaries are two main scattering sources in transparent ceramics, suggesting the presence of many residual pores in the Yb: SrF₂ ceramics. The irregular shape and nonuniform size of the precursor nanopowders favors the generation of residual pores by increasing the amount of compaction defects; therefore, further work needs to be performed to modify the microstructure of the Yb: SrF₂ precursor nanopowders [15,24].

Fig. 4 shows FE-SEM micrographs of the fracture surface of Yb: SrF₂ transparent ceramics. All ceramics have dense microstructures with grain sizes of about 200–500 nm, and the fracture model was mainly intergranular. With increasing Yb³⁺ doping concentration, the grain size gradually decreased, and transgranular cracking became more prominent in the Yb: SrF₂ ceramics. The changing fracture mode indicates that the strength of the grains decreased with increasing Yb³⁺ content, which may have originated from the increased number of residual pores in the grains internal.

The room-temperature absorption spectra of Yb: SrF₂ transparent

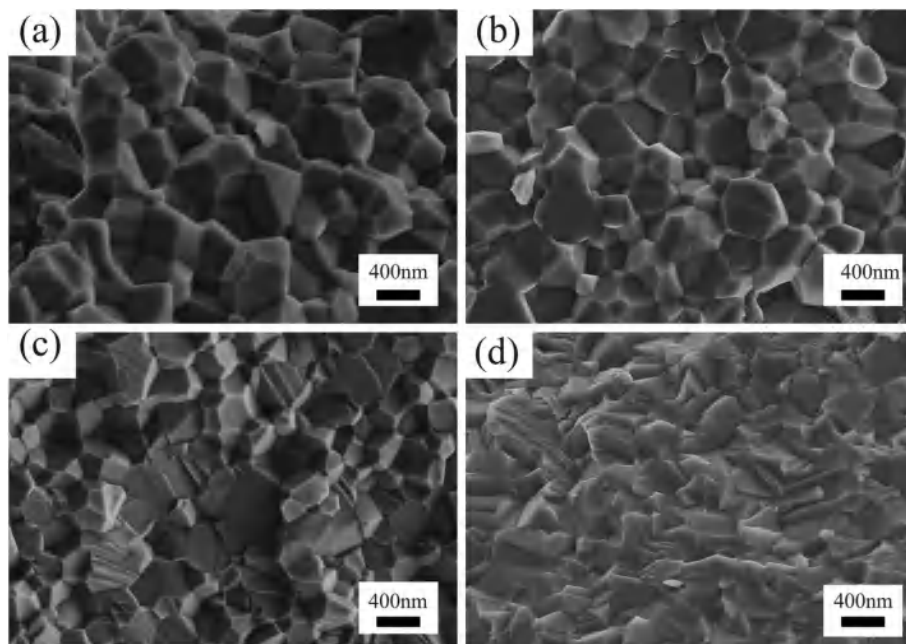


Fig. 4. FE-SEM micrographs of the fracture surfaces of Yb: SrF₂ transparent ceramics with different Yb doping concentrations: (a) 1 at.%, (b) 2 at.%, (c) 3 at.%, and (d) 5 at.%.

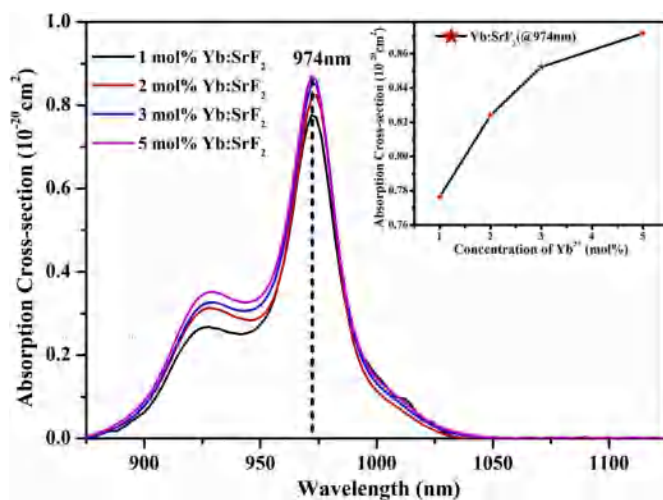


Fig. 5. Absorption spectra of Yb: SrF₂ transparent ceramics with different Yb doping concentrations.

ceramics are shown in Fig. 5, which show that the absorption cross-sections gradually increased with increasing Yb³⁺ doping concentration. The increase in the absorption cross section can be attributed to the local symmetry failure of the crystal as the Yb³⁺ concentration increased, which enhanced the strength of the absorption transition oscillator. All samples displayed similar spectra shapes, which were characterized by a very broad absorption band with a maximum at 973 nm and a shoulder peak at 930 nm. The broad absorption band from 870 to 1040 nm was associated with the electron transition from ground state ²F_{7/2} to the excited state ²F_{5/2} of the Yb³⁺ ion. The appearance of two component peaks in the band was due to Stark splitting of the ²F_{7/2} and ²F_{5/2} energy levels [5,25,26]. Fig. 5 shows that the maximum absorption cross-section of Yb: SrF₂ ceramics at 974 nm was 0.87×10^{-20} cm², which is similar to the single crystal value of Yb: SrF₂ reported by Camy et al. [32].

Fig. 6 shows the room-temperature fluorescence spectra of Yb: SrF₂ transparent ceramics with different Yb³⁺ doping concentrations. Due to

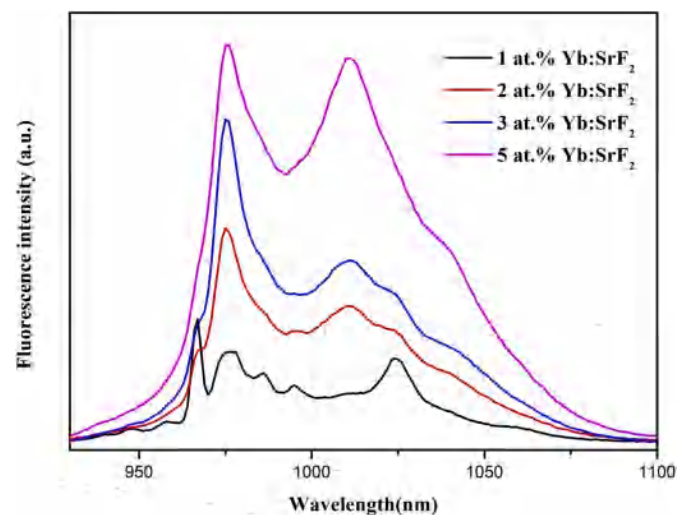


Fig. 6. The emission spectra of Yb: SrF₂ transparent ceramics with different Yb doping concentrations.

Stark splitting, the ²F_{5/2} → ²F_{7/2} emission band transition consisted of several component peaks [5,26,27]. For 1 at.% Yb: SrF₂, the emission band contained five obvious peaks located at 967, 975, 986, 995, and 1024 nm. For 2 at.% Yb: SrF₂, the emission peaks at 967, 986, and 995 nm nearly disappeared, and the intensity of the peak at 1024 nm decreased, while a new peak at 1011 nm began to appear. The emission peak shape of 3 at.% Yb: SrF₂ and 5 at.% Yb: SrF₂ ceramics were nearly identical to the 2 at.% Yb: SrF₂ spectrum but were different from the 1 at.% Yb: SrF₂ sample. The evolution of the emission spectra with increasing Yb³⁺ content was consistent with the spectral behaviors of the transition from individual luminescent centers to hexamer clusters reported by Petit et al. [30]. As can be seen in Fig. 6, the emission intensity increased with increasing Yb³⁺ doping concentration. The luminescence intensity of activated ions is closely related to their doping concentration. Thus, as the Yb³⁺ ion doping concentration increased, the number of luminescent centers increased, and more photon emission

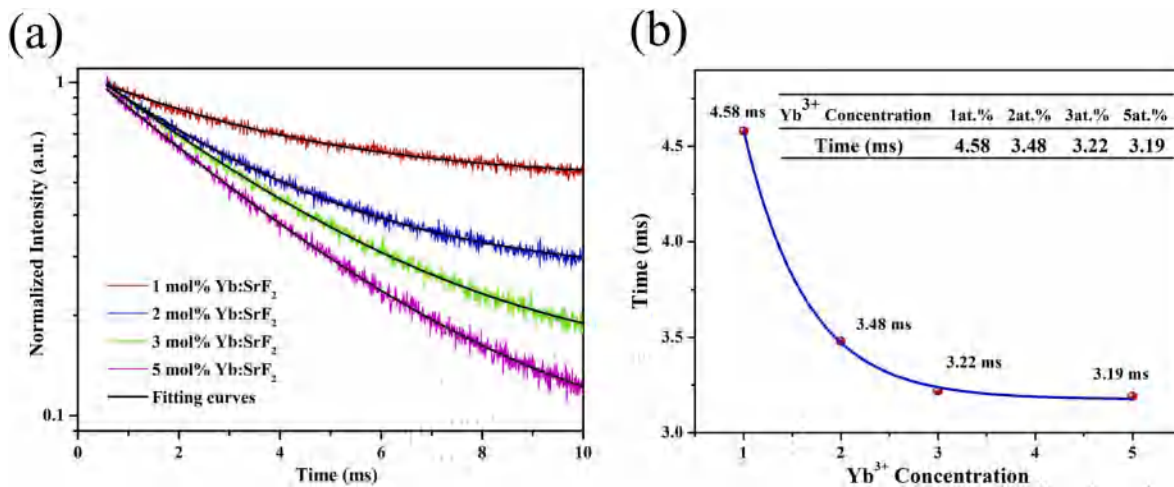


Fig. 7. (a) Decay curves and (b) luminescence lifetimes of Yb: SrF₂ transparent ceramics with different Yb doping concentrations.

increased the fluorescence intensity. On the other hand, the local asymmetry around Yb³⁺ ions increased with increasing Yb³⁺ content. Moreover, with increasing Yb³⁺ content, the peak at 1011 nm became more prominent while the peak at 1024 nm was gradually weakened. The FWHM of the 1011 nm emission for 5 at.% Yb: SrF₂ ceramic reached 63.06 nm, which is higher than the values reported in other papers [27–29]. Yb: SrF₂ ceramics have very broad bandwidths, making them promising materials for generating ultra-short laser pulses.

Fig. 7 shows the luminescence decay curves of Yb: SrF₂ transparent ceramics. Samples were pumped by an 896 nm Xe lamp, and the luminescence decay were recorded at 1011 nm. All decay curves were well fit by a single-exponential function:

$$I(t) = \alpha_1 \exp(-t/\tau_1) + I_0 \quad (2)$$

where t is time, $I(t)$ and I_0 represent the luminescence intensities at t and $t = 0$, α_1 is a constant, and τ_1 is the fitted decay time.

The measured lifetimes for 1, 2, 3, and 5 at.% Yb: SrF₂ transparent ceramics were 4.58, 3.48, 3.22, and 3.19 ms, respectively. Yb: SrF₂ possesses a longer lifetime than that of Yb:CaF₂ (2.4 ms) reported by A. L. et al. [33] which is beneficial for energy storage, making Yb: SrF₂ ceramics suitable for high-power laser output. The luminescence lifetimes versus Yb³⁺ doping concentration are plotted in Fig. 7b. In this study, the lifetime decreased when the Yb³⁺ concentration was increased from 1 to 5 at.%. Incorporating Yb³⁺ resulted in lattice distortion and a reduction in the local symmetry around the Yb³⁺ optical centers, which increased the fluorescence intensity and shortened the lifetime [1]. In addition, the high doping amounts of Yb³⁺ in the SrF₂ lattice led the Yb³⁺ ions to cluster with each other. The Yb³⁺ ions in the clusters have a strong cooperative luminescence effect that can also shorten the fluorescence lifetime [31].

4. Conclusion

Yb: SrF₂ nanoparticles doped with 1–5 at.% Yb³⁺ were prepared by a wet chemical co-precipitation method. The obtained nanoparticles retained the phase structure of SrF₂, and the particle size was about 18–30 nm. Utilizing the synthesized SrF₂ nanoparticles as raw materials, Yb: SrF₂ transparent ceramics were fabricated via a vacuum hot-pressed sintering method. The highest transmittance at 1200 nm of the obtained Yb: SrF₂ transparent ceramics was 85%. The intensities of the emission peaks increased with increasing Yb³⁺ doping concentration. The measured lifetimes of 1 at.% Yb: SrF₂ transparent ceramics were 4.58 ms, which is beneficial for energy storage and makes Yb: SrF₂ transparent ceramics suitable for high-power laser output.

Author's contributions

Yiwei Gao and Bingchu Mei conceived and designed the study. Yiwei Gao performed the experiments and wrote the paper. Weiwei Li, Zhiwei Zhou, Zuodong Liu reviewed and edited the manuscript. All authors read and approved the manuscript.

Declaration of competing interest

The authors declare that they have no conflicts of interest to this work. We declare that we do not have any commercial or associative interest that represents a conflict of interest in connection with the work submitted.

Acknowledgement

This work was supported by the National Natural Science Foundation of China grant numbers (51902234, 51972245, 51432007) and the Fundamental Research Funds for the Central Universities, China (WUT: 2019IVA065, 2019-zy-007).

References

- [1] F.K. Ma, D.P. Jiang, L.B. Su, et al., Spectral properties and highly efficient continuous-wave laser operation in Nd-doped Sr_(1-x)Y_(x)F_(2+x) crystals, *Opt. Lett.* 41 (2016) 501–503.
- [2] X. Lu, B.X. Jiang, J. Li, et al., Synthesis of highly sinterable Yb:Sc₂O₃ nanopowders for transparent ceramic, *Ceram. Int.* 39 (2013) 4695–4700.
- [3] L. Zhang, W. Pan, J. Feng, Dependence of spectroscopic and thermal properties on concentration and temperature for Yb: Y₂O₃ transparent ceramics, *J. Eur. Ceram. Soc.* 35 (2015) 2547–2554.
- [4] K. Takaichi, H. Yagi, A. Shirakawa, et al., Lu₂O₃:Yb³⁺ ceramics—a novel gain material for high-power solid-state lasers, *Phys. Status Solidi* 202 (2005) 1–3.
- [5] G. Boulon, Why so deep research on Yb³⁺-doped optical inorganic materials, *J. Alloys Compd.* 451 (2008) 1–11.
- [6] M. Siebold, S. Bock, U. Schramm, et al., Yb: CaF₂—a new old laser crystal, *Appl. Phys. B* 97 (2009) 327–338.
- [7] H. Wang, J. Zhu, Z. Gao, et al., Femtosecond mode-locked Nd:La:CaF₂ disordered crystal laser, *Opt. Mater. Express* 6 (2016) 2184–2189.
- [8] F. Zhang, H.N. Zhang, D.H. Liu, et al., Tunable Nd, La: SrF₂ laser and passively Q-switched operation based on gold nanobipyramids saturable absorber, *Chin. Phys. B* 26 (2017), 024205.
- [9] B.Z. Malkin, A.M. Leushin, A.I. Iskhakova, et al., EPR and optical spectra of Yb³⁺ in CsCdBr₃: charge-transfer effects on the energy-level structure of Yb³⁺ in the symmetrical pair centers, *Phys. Rev. B* 62 (2000) 7063–7070.
- [10] S. Mizuno, H. Ito, K. Hasekawa, et al., Spectroscopic properties of Nd, Er codoped glasses for solar pumped fiber lasers, *Opt. Mater.* 33 (2011) 1958–1963.
- [11] A.A. Babaev, E.M. Zobov, V.V. Sokolov, et al., Photoluminescence and excitation features of Nd³⁺ ions in (La_{0.97}Nd_{0.03})₂S₃:2Ga₂O₃ glasses, *Semiconductors* 36 (2002) 1244–1247.
- [12] T. Rothacher, W. Lüthy, H.P. Weber, Diode pumping and laser properties of Yb:Ho:YAG, *Optic Commun.* 155 (1998) 68–72.

- [13] A.R. Reinberg, L.A. Riseberg, R.M. Brown, et al., GaAs:Si LED pumped Yb-doped YAG laser, *Appl. Phys. Lett.* 19 (1971) 11.
- [14] P. Lacovara, H.K. Choi, C.A. Wang, et al., Room-temperature diode-pumped Yb:YAG laser, *Opt. Lett.* 16 (1991) 1089.
- [15] Z.W. Zhou, W.W. Li, J.H. Song, et al., Synthesis and characterization of Nd³⁺ doped SrF₂ nanoparticles prepared by precipitation method, *Ceram. Int.* 44 (2018) 4344–4350.
- [16] L. Wei, H. Han, W. Tian, et al., Efficient femtosecond mode-locked Nd,Y:SrF₂ laser, *APEX* 7 (2014), 092704.
- [17] P. Dorenbos, H.W. den Hartog, Space charges and dipoles in rare-earth-doped SrF₂, *Phys. Rev. B* 31 (1985) 3932–3938.
- [18] S.A. Payne, J.A. Caird, L.L. Chase, et al., Spectroscopy and gain measurements of Nd³⁺ in SrF₂ and other fluorite-structure hosts, *J. Opt. Soc. Am. B* 8 (1990) 726–740.
- [19] X. Hu, Q. Yang, C. Dou, et al., Fabrication and spectral properties of Nd³⁺ doped yttrium lanthanum oxide transparent ceramics, *Opt. Mater.* 30 (2008) 1583–1586.
- [20] T. Mioduski, G. Cezary, Z. Dewen, IUPAC-NIST solubility data series. 87. Rare earth metal chlorides in water and aqueous systems. Part 3. Heavy lanthanides (Gd–Lu), *J. Phys. Chem. Ref. Data* 38 (2009) 925–1011.
- [21] J.D. Ng, B. Lorber, J. Witz, et al., The crystallization of biological macromolecules from precipitates: evidence for Ostwald ripening, *J. Cryst. Growth* 168 (1996) 50–62.
- [22] W. Li, B. Mei, J. Song, et al., Fabrication and optical property of highly transparent SrF₂ ceramic, *Mater. Lett.* 159 (2015) 210–212.
- [23] A. Krell, T. Hutzler, J. Klimke, Transmission physics and consequences for materials selection, manufacturing and applications, *J. Eur. Ceram. Soc.* 29 (2009) 207–221.
- [24] X. Xu, X. Sun, H. Liu, et al., Synthesis of monodispersed spherical yttrium aluminum garnet (YAG) powders by a homogeneous precipitation method, *J. Am. Ceram. Soc.* 95 (2012) 3821–3826.
- [25] L. Zhang, Y. Xia, X. Shen, et al., Investigations on the effects of the Stark splitting on the fluorescence behaviors in Yb³⁺-doped silicate, tellurite, germanate and phosphate glasses, *Opt. Mater.* 75 (2018) 1–6.
- [26] T. Kallel, M.A. Hassairi, M. Dammrk, et al., Spectra and energy levels of Yb³⁺ ions in CaF₂ transparent ceramics, *J. Alloys Compd.* 584 (2014) 261–268.
- [27] F. Zhang, J. Liu, W. Li, et al., Dual-wavelength continuous-wave and passively Q-switched Nd,Y:SrF₂ ceramic laser, *Opt. Eng.* 55 (2016) 106–114.
- [28] V. Kubeček, M. Jelínek, M. Čech, et al., Diode-pumped mode-locked operation of a Nd,Y-codoped:SrF₂ Laser, *Opt. Quant. Electron.* 48 (2016) 264.
- [29] X. Xie, B. Mei, J. Song, et al., Fabrication and spectral properties of Nd,La:CaF₂ transparent ceramics, *Opt. Mater.* 76 (2018) 111–116.
- [30] V. Petit, J.L. Doualan, P. Camy, et al., Spectroscopy of Yb³⁺:CaF₂ from isolated centers to clusters, *Phys. Rev. B* 78 (2008) 1–12.
- [31] T. Aidilibike, X. Liu, Y. Li, et al., Structural destruction of cooperative luminescence-A new mechanism of fluorescence quenching, *Opt. Mater.* 69 (2017) 1–7.
- [32] P. Camy, J.L. Doualan, A. Benayad, et al., Comparative spectroscopic and laser properties of Yb³⁺-doped CaF₂, SrF₂ and BaF₂ single crystals, *Appl. Phys. B* 89 (2007) 539–542.
- [33] A. Lyberis, A.J. Stevenson, A. Sukanuma, et al., Effect of Yb³⁺ concentration on optical properties of Yb: CaF₂ transparent ceramics, *Opt. Mater.* 34 (2012) 965–968.